TEARING MODE STABILITY FOR ARBITRARY CURRENT DISTRIBUTION

W. Kerner and H. Tasso

IPP 1/188
IPP 6/205

March 1981

MAX-PLANCK-INSTITUT FÜR PLASMAPHYSIK

8046 GARCHING BEI MÜNCHEN

MAX-PLANCK-INSTITUT FÜR PLASMAPHYSIK

GARCHING BEI MÜNCHEN

TEARING MODE STABILITY FOR ARBITRARY CURRENT DISTRIBUTION

W. Kerner and H. Tasso

IPP 1/188
IPP 6/205

March 1981

- To be published in

PLASMA PHYSICS -

Die nachstehende Arbeit wurde im Rahmen des Vertrages zwischen dem Max-Planck-Institut für Plasmaphysik und der Europäischen Atomgemeinschaft über die Zusammenarbeit auf dem Gebiete der Plasmaphysik durchgeführt.

Tearing Mode Stability for Arbitrary Current Distribution

W. Kerner and H. Tasso

Max-Planck-Institut für Plasmaphysik, D-8046 Garching

EURATOM - Association

Abstract

The linear tearing mode stability is evaluated for 1D equilibria in cylindrical geometry with arbitrary current profiles. This treatment combines the energy method and the Ritz-Galerkin procedure using finite elements. Particularly for hollow currents with two singular q surfaces extremely accurate results showing the coupling influence of both singularities are obtained.

1. Introduction

A major problem in tokamak discharges is the stability of resistive perturbations. In this class the most dangerous ones seem to be tearing modes, which cause the plasma to break away from the magnetic field. This unfreezing of the plasma from the field takes place if the perturbation follows the field line at resonant surfaces. A rigorous formulation of the linear stability of a plasma fluid with respect to resistive modes is given by applying the energy method as shown in Ref. /1/. The question of stability can be decided from a Hermitian eigenvalue problem - as in the case of ideal MHD / 2/ - for which powerful numerical techniques /3/ exist. This energy method holds for configurations with arbitrary cross-sections in the usual tokamak ordering. The perturbation has a multihelical character linearly coupling single helicities at resonant surfaces through the two-dimensionality of the equilibrium. A general 2D stability code is at present being developed. The inclusion of several singular surfaces instead of only one is a crucial step in this program.

In this paper the numerical minimization of the energy functional is restricted to cylindrical equilibria with circular flux surfaces but with arbitrary current profiles which are bell-shaped and, in particular, have dips and holes /4/. Our treatment combines the energy method and the finite-element representation of the perturbation, as already used in ideal MHD (see, for example, /3/)tokamak codes. It is emphasized that the principal value of the energy integral at the singularities, as introduced in /1/ and /5/, is evaluated analytically and thereby kept out of the computation. The basic result of this paper, apart from easily and accurately reproducing known results for bell-shaped currents /6-8/, is that it affords precise numerical investigation of radially coupled perturbations. This happens when the safety factor has the same rational value at different radial points in the plasma column, e.g. for hollow current profiles. The rigorous treatment of several singular surfaces in the perturbation is an important new result.

The tearing mode stability in cylindrical geometry has been investigated before, as can be seen from the literature /6,7,8/, where the shooting technique is applied. This method /6-8/ consists in matching a regular solution for the radial displacement with

the singular solution around a rational q-surface. This, in our opinion, is not suitable for several singular q-surfaces. The initial value scheme for stability as applied in /9/ is presumably not suitable for very weak resistivities as in high-temperature plasmas and the accuracy may be questionable if the number of tearing layers is large as in the case of shaped cross-section tokamaks.

The plan of the paper is as follows: Section II formulates the problem and describes the method of solution. The results are presented in Sec. III and finally discussed in Sec. IV.

II. Method

We consider resistive systems in a static equilibrium. The equilibrium magnetic field B and current density J are given by

$$\underset{\sim}{B} = \nabla z \times \nabla \psi + B_z \nabla z \tag{1}$$

$$\underset{\sim}{j} = j(\psi) \nabla z = \frac{1}{\mu_0} \nabla \times \underset{\sim}{B}$$

where ∇z is the unit vector along the plasma column with length L . The poloidal flux ψ satisfies the equilibrium equation

$$\frac{1}{\mu_0} \nabla^2 \psi = j(\psi) = - \frac{dp_0}{d\psi} \tag{2}$$

with an arbitrary pressure profile $p_0(\psi)$. Moreover, B_z and the electric field

$$\underset{\sim}{E} = \eta_0 \underset{\sim}{j} = \eta_0(\psi)\, j(\psi) \nabla z \tag{3}$$

where η_0 is the resistivity, are constants in the equilibrium. The equilibrium quantities are represented either as polynomials or as pointwise data. For

$$j(\psi) = \sum_{i=0}^{N} c_i r^i$$

we obtain from eq. (2)

$$\psi(r) = \mu_0 r^2 \sum_{i=0}^{N} \frac{c_i}{(i+2)^2} r^i \tag{4}$$

For pointwise given profiles, especially for experimentally given ones, the current density is interpolated by cubic splines from which the other equilibrium quantities are exactly calculated.

The linearized stability equations are derived in /1/ on the assumptions of incompressibility, transport of resistivity by magnetic surfaces, and tokamak ordering. Minimization of the energy

$$\delta W = \int d\tau \left\{ \frac{1}{\mu_0} |\nabla_\perp A|^2 + A^* \frac{dj(\psi)}{d\psi} (A - \tilde{A}) \right\} \tag{5}$$

with the constraint $\int |A|^2 d\tau = c\ell.$

leads to the Euler equation

$$-\frac{1}{\mu_0} \nabla_\perp^2 A + \frac{dj}{d\psi} (A - \tilde{A}) = \lambda A \tag{6}$$

where A is the z component of the vector potential of the perturbed field and $\tilde{A}$ is the weighted surface average of A. The chosen norm ensures a finite energy of the magnetic perturbation. Mathematically, the use of the L^2 norm is allowed due to the fact that the solutions of the Euler equation behave near singular surfaces like $x \ln|x|$ so that for a finite domain the solution will be finite everywhere if it is finite at one point.

The sign of λ governs stability.

In the case of a Fourier expansion for A in a flux coordinate system ψ, θ, z

$$A(\psi, \theta, z) = \sum_m a_m(\psi)\, e^{i(m\theta + n 2\pi z/L)} \tag{7}$$

$\tilde{A}$ is given by

$$A - \hat{A} = \sum_m \frac{m}{n\, q(\psi) + m}\, a_m(\psi)\, e^{i(m\theta + n 2\pi z/L)} \tag{8}$$

where the surface quantity q denotes the safety factor. For 1D cylindrical geometry - as assumed in this paper - the different harmonics in the series (7) decouple. A is taken to be zero at the plasma boundary. In order to simulate a plasma-vacuum-wall system within this theory one need only make the resistivity very large and hence the current very small in the "vacuum" region.

The extremum of δW is evaluated by means of the Galerkin form, where A is expanded into finite elements

$$(9) \qquad A(\psi, \theta, z) = \sum_m e^{i(m\theta + i 2\pi n z/L)} \sum_{\nu=1}^{M} \alpha_\nu^m e_\nu^m(\psi)$$

with constants α_ν^m, leading to a matrix eigenvalue problem

$$(10) \qquad (M)\ \underset{\sim}{\alpha} = \lambda\ (N)\ \underset{\sim}{\alpha}$$

In the usual cylindrical coordinate system r, θ, z the matrix elements of the potential and kinetic-like energy matrices are given by

$$M_{\nu,\nu'}^m = \int_0^a dr \Big[\frac{d\chi}{dr} \frac{m q(r)}{n q(r) + m} e_\nu^m e_{\nu'}^m + r \left(\partial/\partial r\, e_\nu^m\right)\left(\partial/\partial r\, e_{\nu'}^m\right) + m^2 1/r\ e_\nu^m e_{\nu'}^m \Big] \qquad (11)$$

$$(12) \qquad N_{\nu,\nu'}^m = \int_0^a r\, dr\, e_\nu^m e_{\nu'}^m ,$$

where r = 0 denotes the position of the plasma centre, and r = a the plasma boundary. Note that the energy matrix has singularities at singular surfaces, $r = s_i$

$$(13) \qquad n q(s_i) + m = 0$$

There the integrals are evaluated as principal parts.

On the assumption of a non-vanishing gradient of the safety factor at the singular surfaces

$$(14) \qquad \frac{dq(s_i)}{dr} = q'(s_i) \neq 0 \qquad \text{for all } i,$$

all integrals then have a finite value. It should be emphasized that the condition (14) is practically non-restrictive since the q profile can be shifted a little so that eq. (14) is satisfied.

The applied finite elements are of the lowest degree compatible with the integrals, i.e. linear elements. These functions are continuous and differentiable but the derivatives have jumps and are defined as follows:

$$(15)\qquad e_\nu^m(r) = \begin{cases} (r - r_{\nu-1}) / (r_\nu - r_{\nu-1}) & r_{\nu-1} \le r \le r_\nu \\ (r_{\nu+1} - r) / (r_{\nu+1} - r_\nu) & r_\nu \le r \le r_{\nu+1} \\ 0 & r \notin [r_{\nu-1}, r_{\nu+1}] \end{cases}.$$

The boundary conditions on A lead to $\alpha_1^m = \alpha_M^m = 0$.

Near singular surfaces the function A exhibits logarithmic-type behaviour. It also has a steep gradient which is best represented by the elements defined in eq. (15). The evaluation of the principal part around the singularities is done as follows: For an integrand of the form $f(r)/(nq+m)$, where $f(r)$ is regular, we define

$$(16)\qquad \bar{I}(r) = \frac{f(r)}{nq+m} - \sum_{i=1}^{N_s} \frac{f(s_i)}{nq'(s_i)(r-s_i)}$$

where $\bar{I}(r)$ is continuous across all singular surfaces. The principal value of the second term is obviously a logarithm. This allows to compute $P\int \frac{f(r)\,dr}{(nq+m)}$ in terms of $\int \bar{I}(r)\,dr$ and logarithms near the singularities. For numerical convenience the mesh points r_j are chosen not to coincide with the s_i, $r_j \neq s_i$ for all j and i . Large cancellations of the different terms in $\bar{I}(r)$ (eq.(16)) for $r \approx s_i$ are avoided by further expanding q(r) and f(r). For example, one gets

$$(17)\qquad (nq+m)^{-1} - (nq'(s_i)(r-s_i))^{-1} \longrightarrow -\frac{1/2\, q''(s_i)}{n(q'(s_i))^2}$$

if $|r - s_i| < \epsilon$.

By these procedures all matrix elements can be easily and accurately computed by using a four-point Gaussian quadrature. The choice of linear finite elements leads to tridiagonal matrices $M_{\nu,\nu'}$ and $N_{\nu,\nu'}$, where M and N are non-zero only if $\nu' = \nu, \nu \pm 1$.
The lowest N_L eigenvalues together with the eigenfunctions are computed by using the package SIVI /10/.

It is emphasized that the lowest eigenvalue in the system is always approximated from

above as the number of finite elements is increased. By means of a convergence study $\lambda = \lambda(N_r)$ with extrapolation for λ to an infinitely dense mesh, the question of stability is decided with extremely high accuracy.

Finally, let us remark that a real physical growth rate $\Lambda = \Lambda(\lambda)$ remains undetermined and would require additional analysis.

III. Results

a) One singular surface

First we want to demonstrate the capability of our code by reproducing known results for monotonically decreasing current profiles. The equilibria of the form

$$j(r) = j_o (1 - r^2/a^2)^{\mu} \qquad \mu = 1, 2, \ldots \tag{18}$$

with

$$q(a) / q(0) = \mu + 1$$

are dealt with in, for example, Ref. /6/.

We confirm that there is always a m = 1 tearing mode instability if the q = 1 surface is located in the plasma, which can be avoided by choosing q (r=0) greater than one. We also find that the most dangerous modes are then the m = 2 and 3 perturbations. For m = 2 the marginal points with respect to stability are q(o) = 2.0 and $q(a) = q_a(\mu)$, in agreement with Fig. 35 of Ref. /6/. These marginal points are easily computed for μ = 1, 2 ... up to 11 using only 40 to 100 radial mesh points, where, for example, a case with q(o) = 1.999 is unstable and one with q(o) = 2.001 is stable. These instabilities can be stabilized by flattening the current around singular surfaces pointwise. Figure 1 shows the current density and safety factor profiles with unstable n = 1, m = 2 and n = 2, m = 3 modes. By changing these profiles as indicated by the dotted lines (Fig. 1) one can achieve stability to all (n,m) modes for n = 1, 2, 3, 4 and m = 1, 2, ...10, independently of the position of the perfectly conducting wall. A typical eigenfunction is displayed in Fig. 2 for an unstable n = 2, m = 3 mode. Its derivative has the maximum value at the singular surface represented by the dotted line.

b) Two singular surfaces

We now discuss configurations with two singular surfaces. This happens for "hollow" temperature and current profiles frequently observed in, for instance, PLT /4/. Such profiles can easily be mocked up by modifying the function in eq. (18) to the form

$$(19) \qquad j = j_0 \left(1 + \beta r^2/q^2\right)\left(1 - r^2/q^2\right)^{\mu} .$$

A pronounced dip at the centre occurs for $\mu = 3$ and $\beta = 10$. These profiles are shown in Fig. 3. From this equilibrium other equilibria are derived simply by multiplying j and ψ by a factor σ, leading to shifted q values but leaving the profile shapes unchanged. The positions of the resonant surfaces, S_1 and S_2, are thereby modified. For $q\,(r = o) = 2.50$ the singular surfaces are located at $r/a = s_1 = 0.30$ and $r/a = s_2 = 0.73$.

For this equilibrium there exist two unstable $n = 1$, $m = 2$ modes. The corresponding eigenfunctions are displayed together with their derivatives in Figs. 4a) and 4b). These figures show finite values for the eigenfunctions between S_1 and S_2 and steep gradients at S_1 and S_2, which means strong radial coupling due to the two singularities. The most unstable mode has a minimum between S_1 and S_2, whereas the second unstable mode changes its sign as is to be expected. The contributions to the energy δW come in both cases especially from the regions near the two singular surfaces.

In order to understand this coupling in more detail, let us change the scaling factor σ and label different equilibria by their q value on axis, q_o. Increasing q_o above 1.5, the $q = 2$ surface enters the plasma from the boundary $r = a$. This configuration is stable owing to the proximity of the resonant surface to the boundary, which has a stabilizing effect in δW through the term $|\nabla_\perp A|^2$. It turns out that an unstable mode can develop only if q_o is greater than 1.73 with $S_2 < 0.93$, the corresponding eigenfunction being concentrated around S_2. By increasing q_o above 2.0 a singularity S_1 is created close to $r = 0$ and an unstable eigenfunction peaked around S_1 occurs. These two modes,

both of the type of Fig. 2, are decoupled until q_o is increased up to values larger than 2.4. Note that for $q_o \simeq 2.8$ s_1 coincides with a zero of the gradient of the current density, which diminishes the destabilizing influence of the singular surface . Finally, s_1 and s_2 coincide and for $q_o > 2.82$ the instability completely disappears.

c) PLT profiles

A profile with a pronounced current hole in the centre is taken from PLT data. The corresponding q value drops from $q_o = 8.9$ at the centre to below 3 in the middle and then increases again to a value of 4.9 at the surface, as is shown in Fig. 5. This configuration has two unstable n = 1, m = 3 modes. One mode has no radial node and is concentrated around the inner singular surface $s_1 = 0.29$, and the other mode has a radial node and sees both s_1 and s_2 ($s_2 = 0.72$). It is interesting that the small change in the current, indicated by dots in Fig. 5, stabilizes this second mode.

As done before, this equilibrium is changed by a scaling factor σ shifting the position of the resonant surfaces. For q_o between 8.5 and 9.9 there are two unstable n = 1, m = 3 modes. One of them is similar to the mode plotted in Fig. 4a with a somewhat smaller coupling between s_1 and s_2, and the second has the typical shape of the function shown in Fig. 4b. For q_o greater than 9.9 the current gradient at the inner singular surface s_1 becomes smaller and finally vanishes for $q_o = 10.65$. The eigenfunction is everywhere finite and now has no minimum between s_1 and s_2, as shown in Figs. 6a-c. At $q_o = 10.65$ the eigenfunction becomes smooth at s_1, having only one steep gradient at s_2 (see Fig. 6b) instead of two (see Figs. 6a-6c).

In general, the contributions to δW come not only from the regions near the singularities but also from farther regions, as can be seen from Fig. 7. Stability, therefore, cannot be determined by treating singularities independently.

IV. Conclusion

The main achievement of this paper is the elegant and precise numerical treatment of stability of linear tearings with many singularities. This is due to the combination of the energy method and the finite-element representation.

The basic results published on cylindrical tokamaks in the case of bell-shaped current distributions are easily recovered. Particular attention is devoted to current distributions with holes having several singular surfaces of the same rationality as found in some PLT experiments leading to multiply peaked and radially coupled tearings. The stability of which is computed with very high accuracy.

The essentials of this calculation can be extended to the case of shaped cross-sections, the difference being mainly the poloidal coupling of modes. This two-dimensional code should be available soon.

Acknowledgement

The authors appreciate valuable discussions with J.T. Virtamo. They also thank E. Schwarz for her contribution to the code, especially for writing the spline and plot routines.

Figure Captions

Fig. 1 Safety factor q and current density j profiles of an unstable (——) and a stable (----) equilibrium.

Fig. 2 Unstable eigenfunction A (n = 2, m = 3) with one singular surface at $r/a = s_1$

Fig. 3 Safety factor q and current density profile $j = j_o(1 + 10\, r^2/a^2)(1 - r^2/a^2)^3$ with two singular q = 2 surfaces

Fig. 4 Unstable eigenfunction A (n = 1, m = 2) and its derivative dA/dr for the equilibrium shown in Fig. 3, obtained with 200 radial mesh points
a) the most unstable mode ($\lambda = -74.3$)
b) the second unstable mode ($\lambda = -65.7$)

Fig. 5 Safety factor q and current density j taken from PLT data having two (——) and one (----) unstable (n = 1, m = 3) modes

Fig. 6 Unstable eigenfunction A (n = 1, m = 3) and its derivative dA/dr for the dotted equilibrium shown in Fig. 5, obtained with 200 radial mesh points
a) $q_o = 10.0$ ($\lambda = -46.9$)
b) $q_o = 10.65$ ($\lambda = -65.2$)
c) $q_o = 11.30$ ($\lambda = -146.9$)

Fig. 7 Pointwise contributions to the energy obtained with 200 radial mesh points for the PLT equilibrium with $q_o = 11.30$. The index i denotes integration from r_i to r_{i+1} .

References

/1/ Tasso, H., Virtamo, J.T., Plasma Physics 22, 1003 (1980)

/2/ Bernstein, I.B., Frieman, E.A. Kruskal, M.D., Kulsrud, R.M., Proc. Roy. Soc. (London) A224, 17 (1958)

/3/ Gruber, R., Troyon, F., Berger, D., Bernard, L.C., Rousset, S., Schreiber, R., Kerner, W., Schneider, W., Roberts, K.V., Comp. Phys. Comm. 21, 323 (1981)

/4/ Sauthoff, N.R., von Goeler, S., Stodiek, W., PPPL-1379, Princeton, N.J. (1977)

/5/ Tasso, H., "Lectures on Plasma Physics", IFUSP/P-181, LEP-8, Sao Paulo, 1979

/6/ Wesson, J., Nucl. Fusion 18, 87 (1978)

/7/ Glasser, A.H., Furth, H.P., Rutherford, P.H., Phys. Rev. Lett. 38, 234 (1977)

/8/ Lackner, K., F. Karger, 8th Europ. Conf. on Contr. Fusion and Plasma Physics, Prag 1977, Vol. I, 5

/9/ Carreras, B., Hicks, H.R., Waddell, B.V., Nuclear Fusion 19, 583 (1979)

/10/ Gruber, R., Comp.Phys. Comm. 10, 30 (1975)

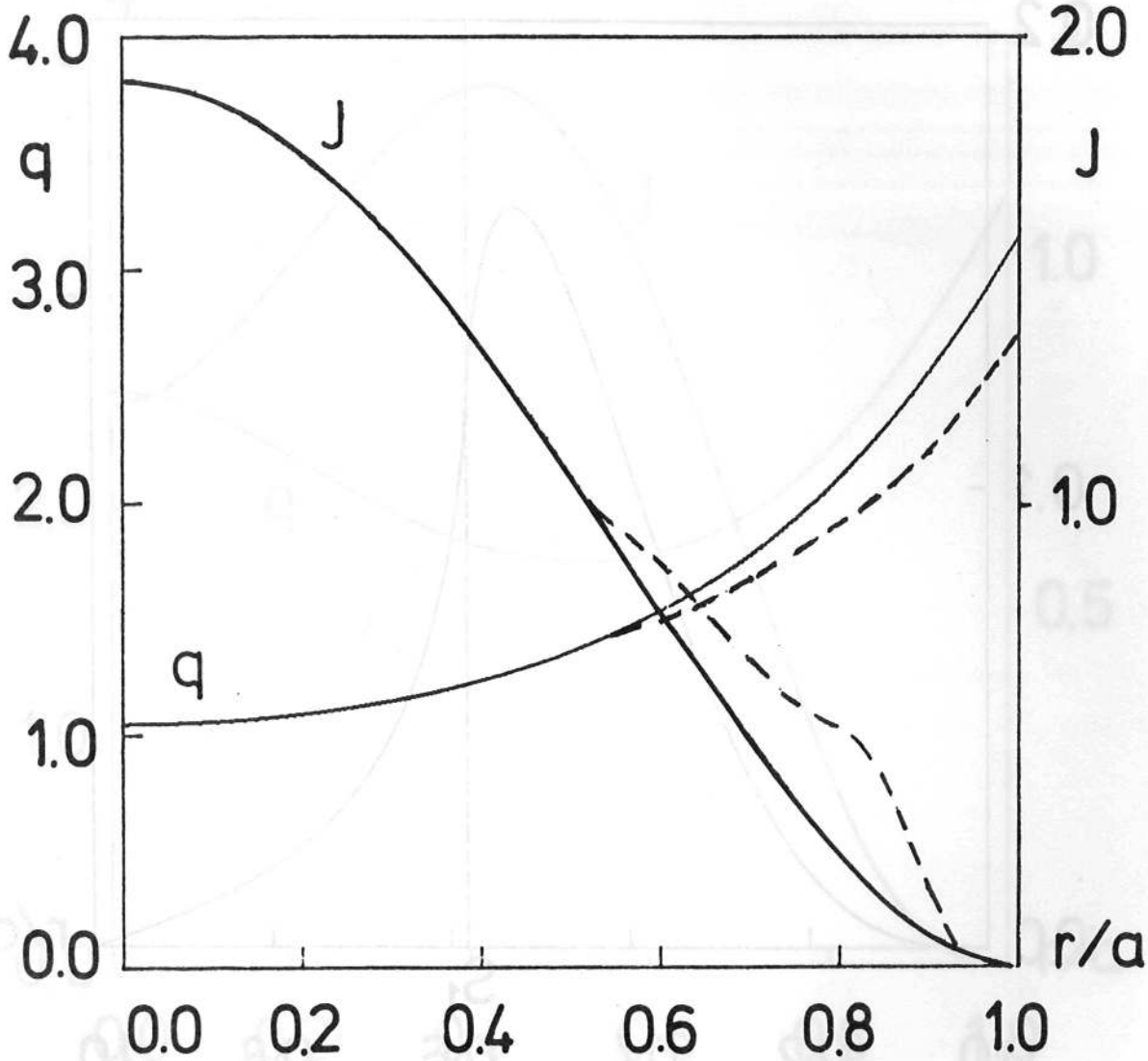

Fig. 1

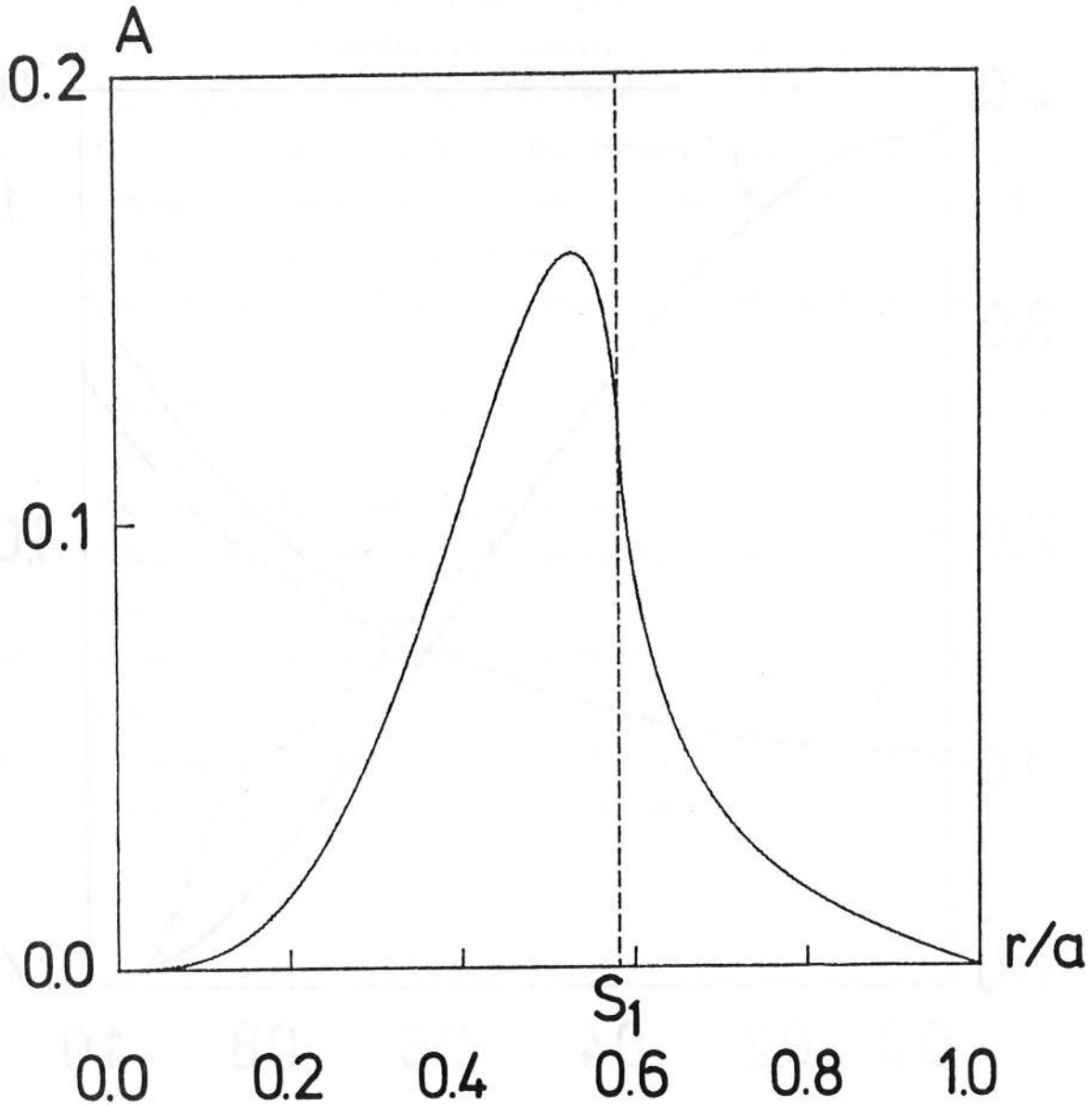

Fig. 2

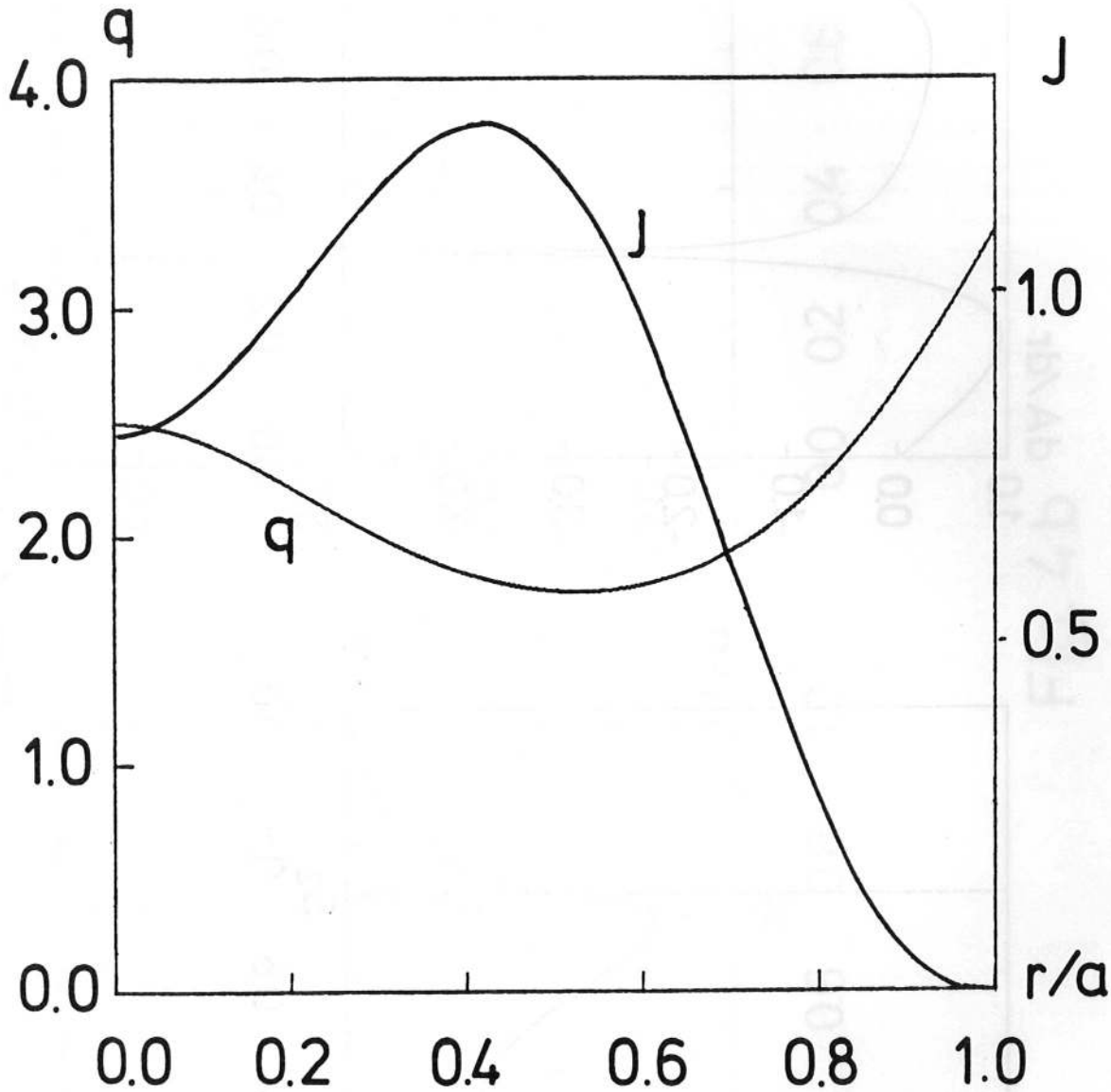

Fig. 3

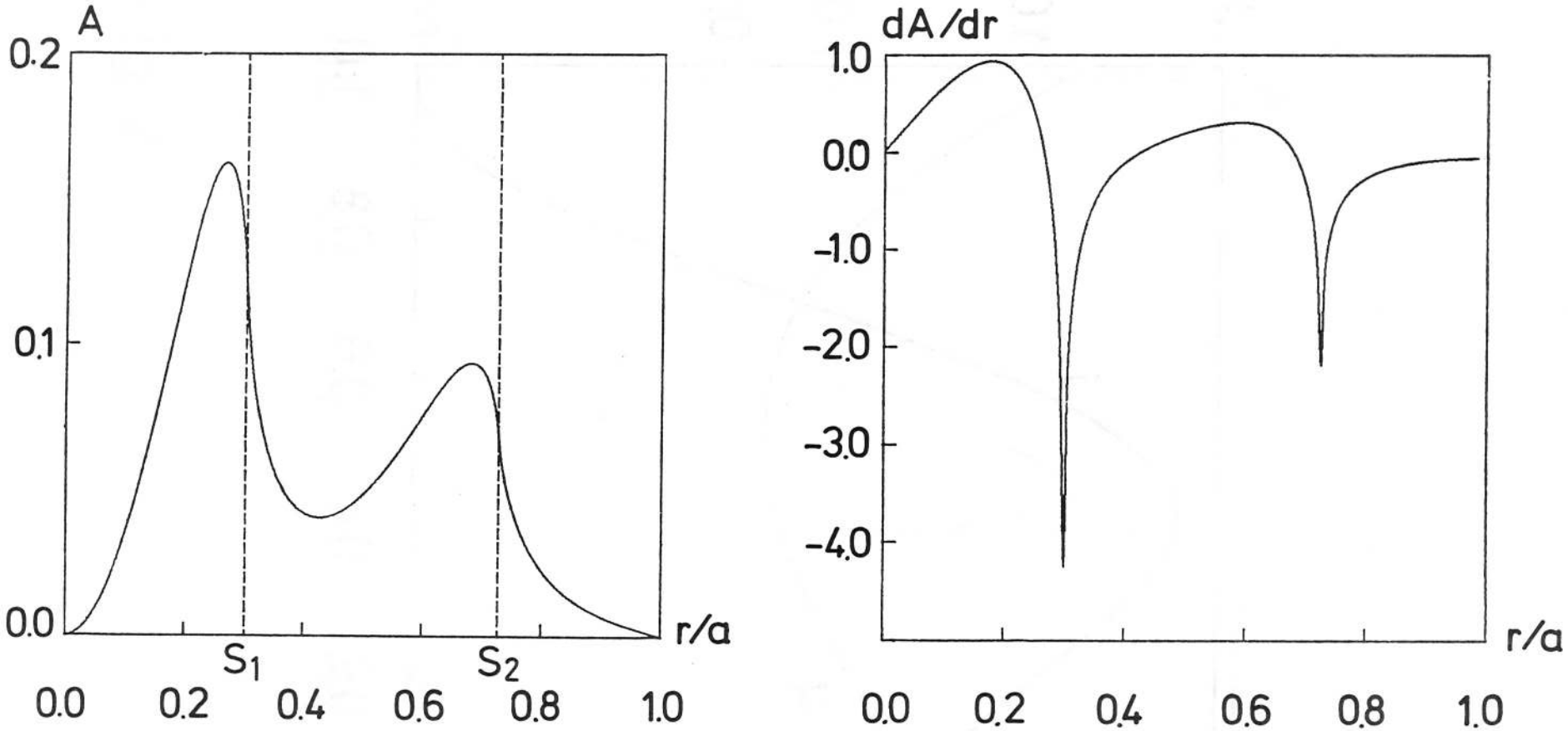
A
0.2
0.1
0.0
r/a
S1
S2
0.0
0.2
0.4
0.6
0.8
1.0
dA/dr
1.0
0.0
-1.0
-2.0
-3.0
-4.0
r/a
0.0
0.2
0.4
0.6
0.8
1.0

Fig. 4 a

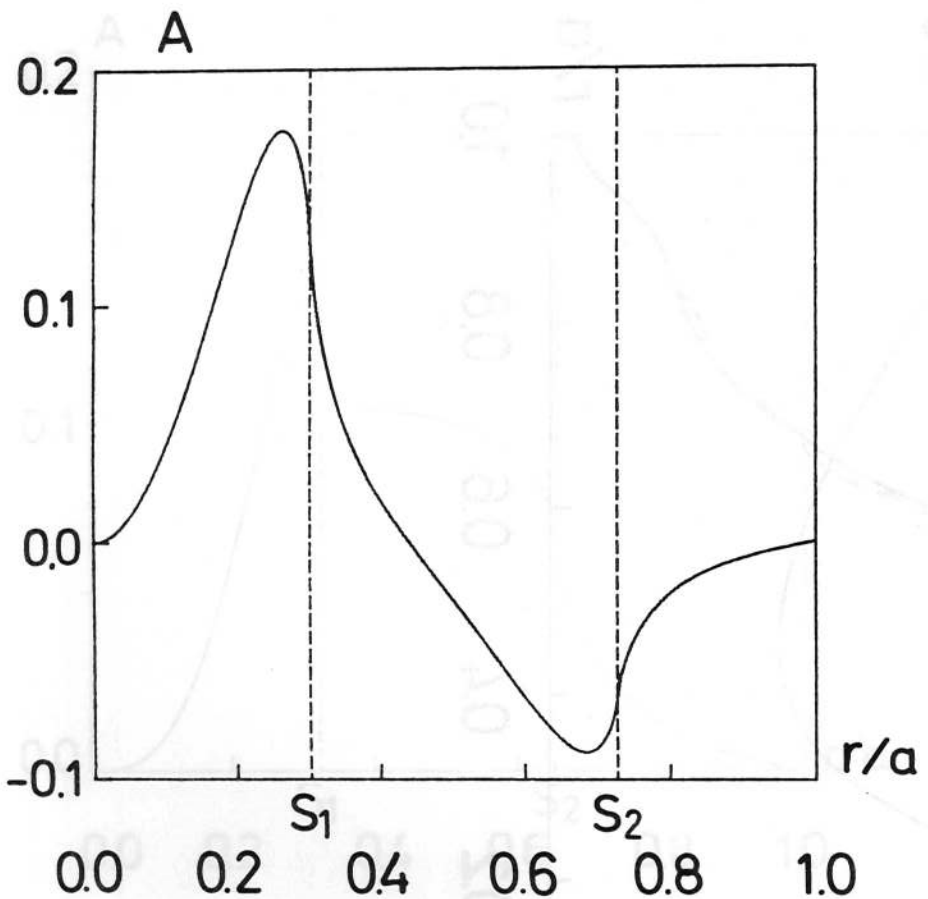
A
0.2
0.1
0.0
-0.1
S1
S2
r/a
0.0
0.2
0.4
0.6
0.8
1.0

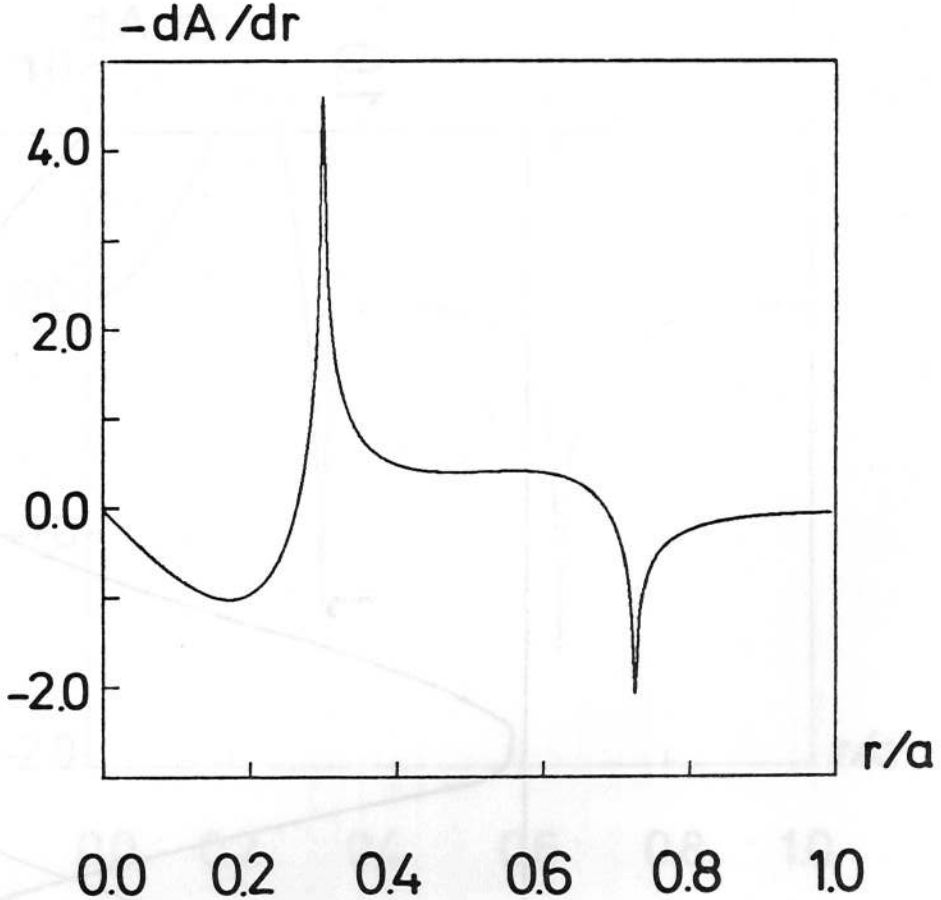
-dA/dr
4.0
2.0
0.0
-2.0
r/a
0.0
0.2
0.4
0.6
0.8
1.0

Fig. 4 b

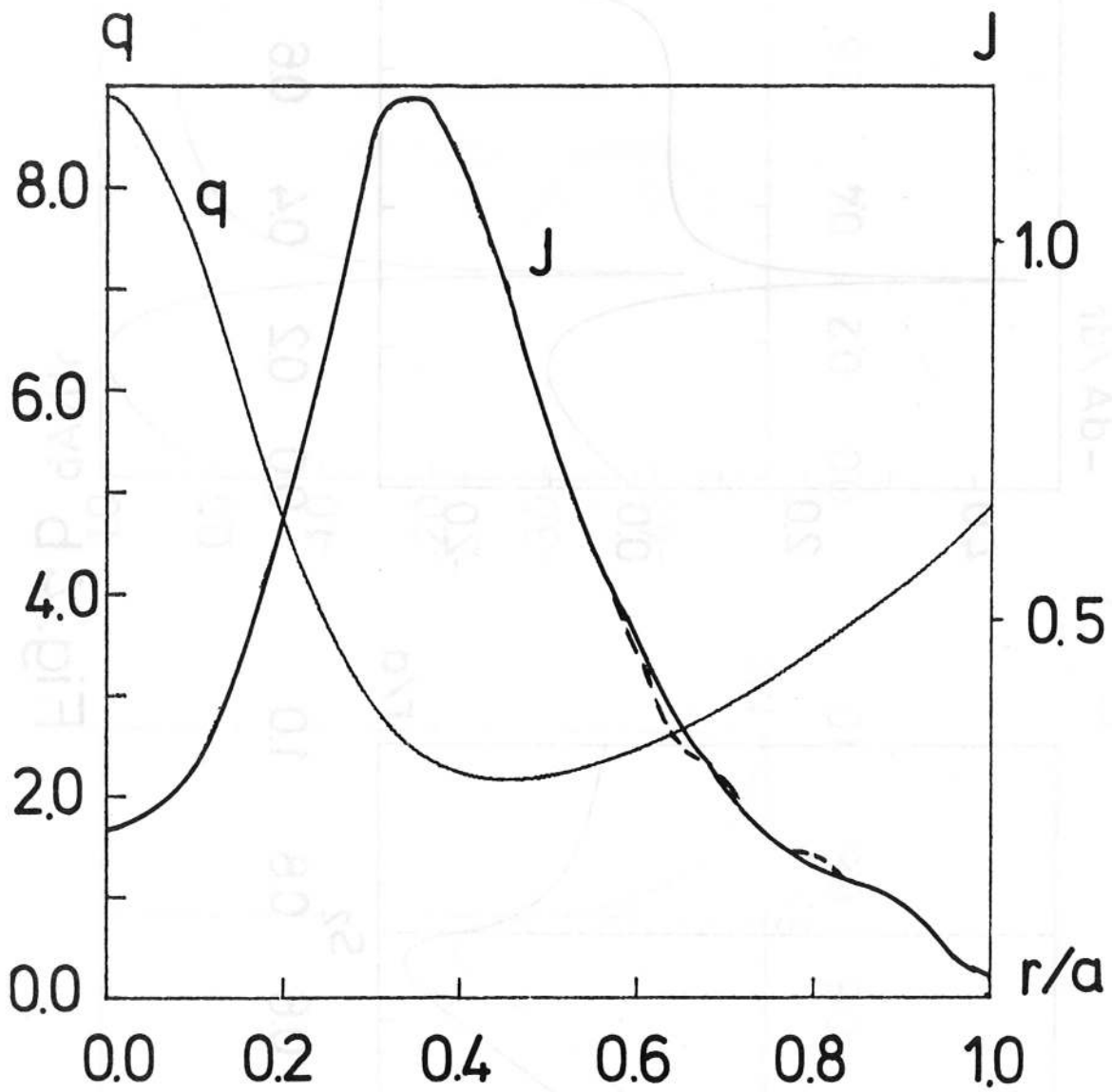

Fig. 5

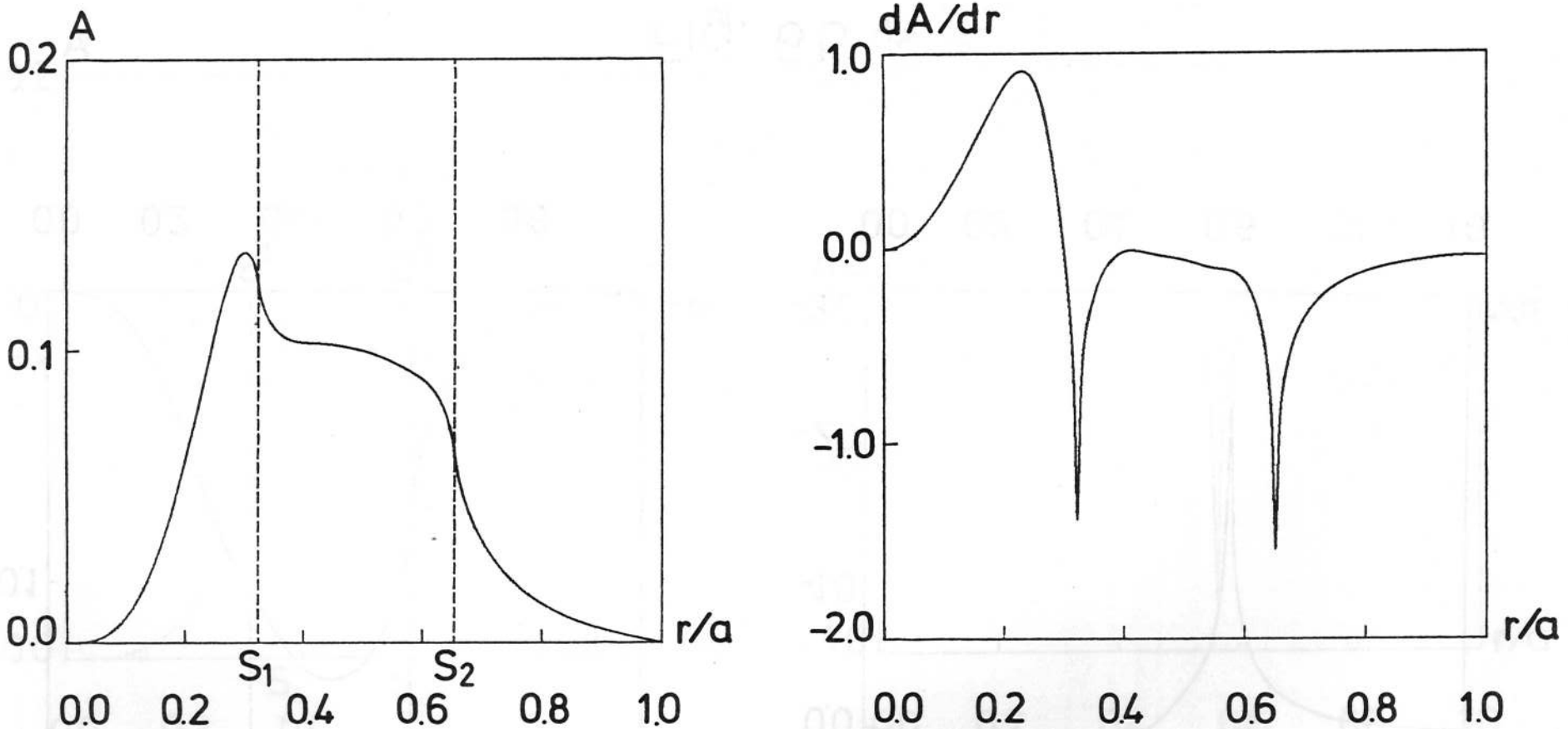
A
0.2
0.1
0.0
r/a
S1
S2
0.0
0.2
0.4
0.6
0.8
1.0
dA/dr
1.0
0.0
-1.0
-2.0
r/a
0.0
0.2
0.4
0.6
0.8
1.0

Fig. 6a

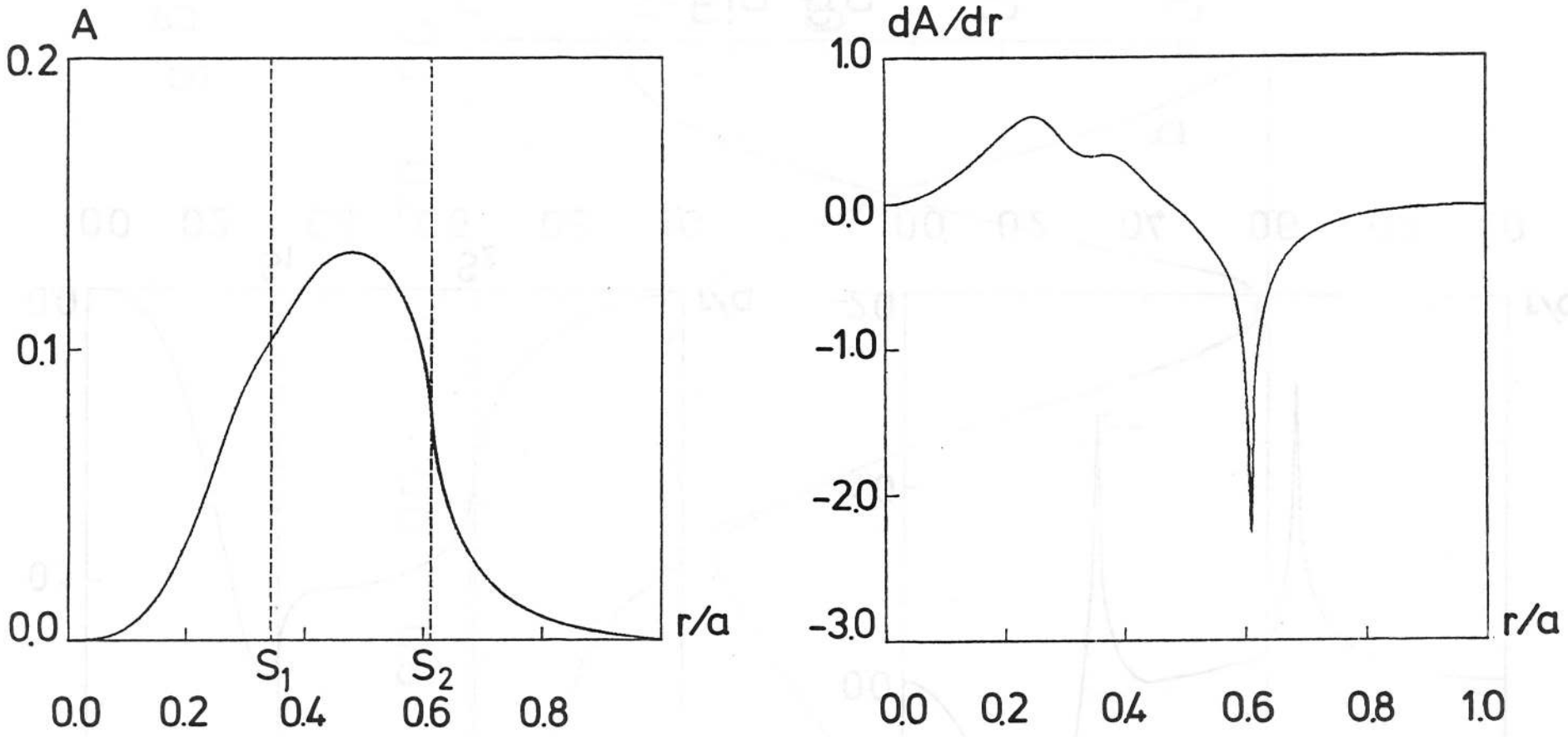
A
0.2
0.1
0.0
S1
S2
0.0
0.2
0.4
0.6
0.8
r/a
dA/dr
1.0
0.0
-1.0
-2.0
-3.0
0.0
0.2
0.4
0.6
0.8
1.0
r/a

Fig. 6 b

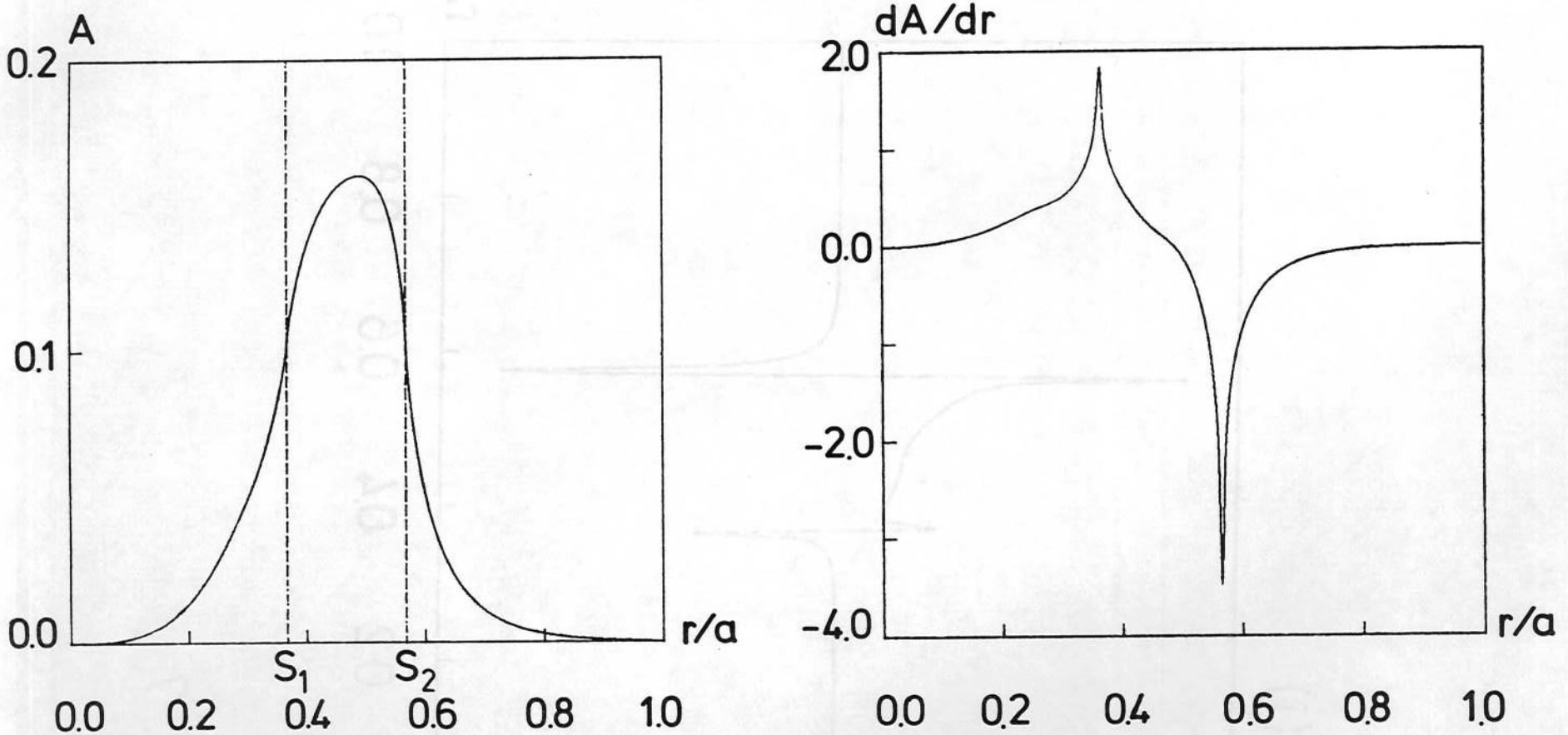
A
0.2
0.1
0.0
r/a
S_1
S_2
0.0
0.2
0.4
0.6
0.8
1.0
dA/dr
2.0
0.0
-2.0
-4.0
r/a
0.0
0.2
0.4
0.6
0.8
1.0

Fig. 6c

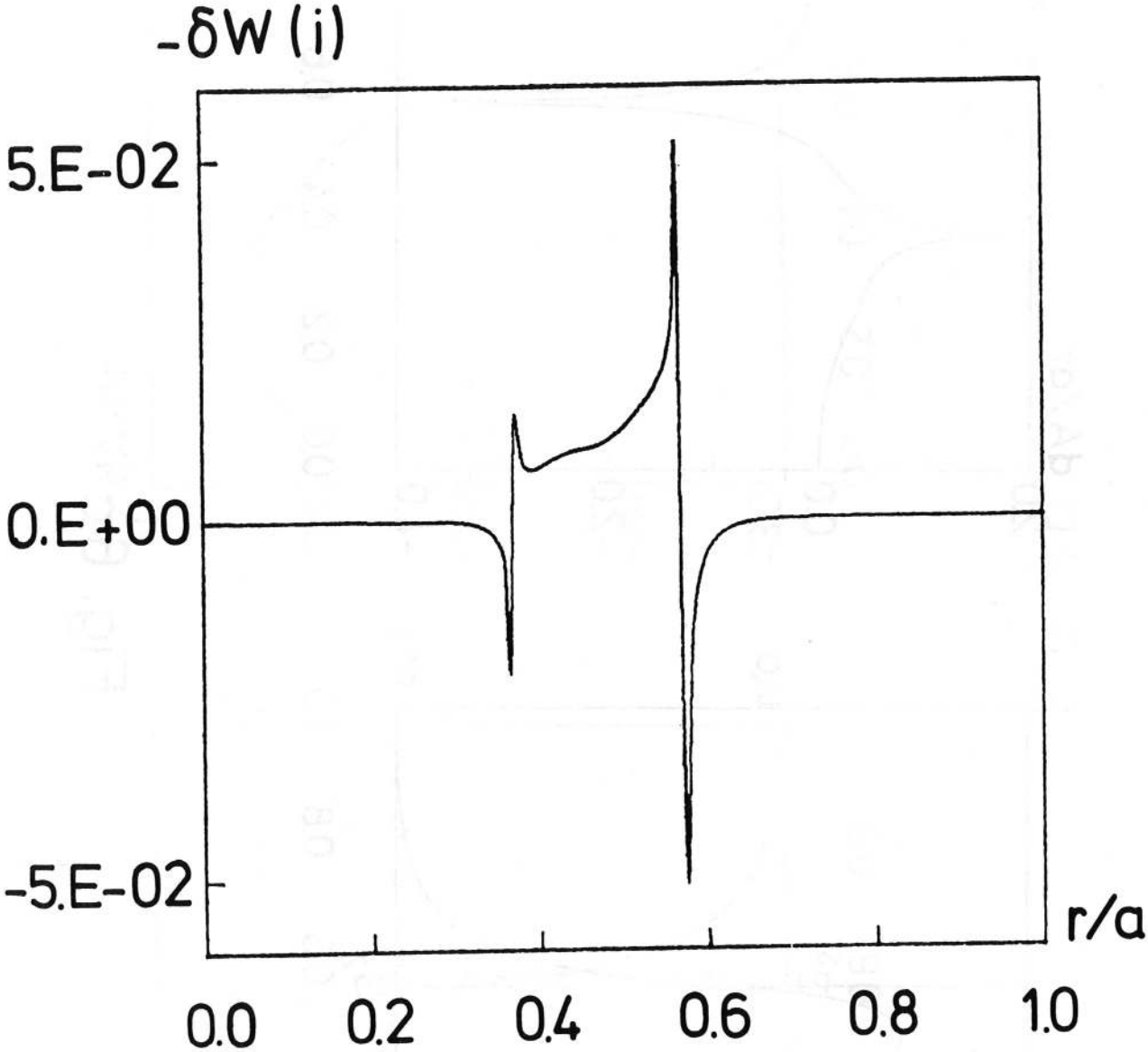

Fig. 7